A High-Precision Motion Control Based on a Periodic Adaptive Disturbance Observer in a PMLSM

Kwanghyun Cho, *Student Member, IEEE*, Jonghwa Kim, Seibum Ben Choi, *Member, IEEE*, and Sehoon Oh, *Member, IEEE*

***Abstract*—This paper presents a novel disturbance compensation scheme to attenuate periodic disturbances on repetitive motion using permanent magnet linear synchronous motors (PMLSMs), and this scheme is called the periodical adaptive disturbance observer. The scheme is based on assumptions that all measured states and disturbances are periodic and repetitive when the tasks executed by PMLSM motion systems have periodic and repetitive characteristics. In the proposed control scheme, a lumped disturbance is estimated by the classical linear disturbance observer (DOB) for the initial time period and stored in memory storages. It consists of parametric errors multiplied by states, friction force, and force ripple, and then, it is updated for each time period by the periodic adaptation law. This scheme requires no mathematical models of disturbances and adaptation laws of model parameters such as the mass of the mover and viscous friction coefficient. Also, it is possible to compensate for disturbances above as well as below the bandwidth of the Q-filter (LPF) of DOB. The effectiveness of the proposed control scheme is verified by various experiments that take into account varying frequency components of disturbances along the operating speed of a mover of PMLSM such as force ripple and friction force.**

***Index Terms*—Adaptation, disturbance observer, (DOB), force ripple compensation, periodic disturbance.**

I. Introduction

As demand increases for high-speed/high-accuracy motion, various types of linear motor-driven motion systems have received significant attention for precision motion control. The motion system based on permanent magnet linear synchronous motors (PMLSMs) is extending steadily to a variety of industrial applications since it has advantages such as high speed/force density and low thermal losses. However, there are still serious problems to achieve high positioning precision control. First, as with other types of the linear motor-driven motion systems, it is sensitive to variations of model parameters such as the mass of the mover and friction coefficients. Second, the friction force on linear motion guides affects the motion system as a dominant disturbance because it varies depending on the operating speed of the mover of a PMLSM and has heavy nonlinearities on low-speed motion. Also, the motion systems based on linear motors using the iron-core like PMLSMs are directly affected by the force ripple that is induced by the attraction between the magnets and the iron-core of the mover. It is a position-dependent periodic disturbance that has the same fundamental period as the pole pitch of permanent magnets. Since the fundamental and harmonic frequencies of the force ripple are increased proportional to the speed of the operating system, it is hard to attenuate them perfectly when the high-speed motions are required. Therefore, these parameter variation and dominant disturbances should be compensated to achieve high-speed/high-positioning precision control in PMLSM motion systems.

Recently, numerous methods have been developed for the compensation of these disturbances in various actuators including linear motors. In [1] and [2], dual-relay feedback approaches based on describing functions were presented to obtain the friction force models and compensate for them. In [3] and [4], nonlinear observer compensation methods using LuGre model were presented to cope with the friction force. In [5], a friction compensation technique based on a projection parameter adaptation for a dynamic friction model was presented. Asymmetric friction model was identified by using the least-square identification method in [6]. In [7], a nonlinear static friction was modeled by the Hsieh–Pan model. In [8], the friction force considered as the unstructured uncertainties was compensated by RISE without the friction force model. In [9] and [10], several schemes were introduced to compensate for the force ripple that is modeled by the Fourier expansion. Here, unknown parameters such as the amplitude and phase of the model were estimated by a certain parameter adaptation mechanism. These methods estimate or compensate for friction force and force ripple separately due to motor types or experimental assumptions. However, it is hard to separate each disturbance in practice due to the effects coupled with states such as position and velocity. In [11]–[15], adaptation laws for the parameters of each model of disturbances were presented to compensate for friction force and force ripple simultaneously, but it is not easy to guarantee asymptotic convergence of estimated parameters in models over various operating conditions. Unlike stated methods, some schemes that require no disturbance models exist. A disturbance observer (DOB) estimates and attenuates a lumped disturbance by using the difference between the output of the inverse nominal model and the control input [16]–[18]. However, the use of

Manuscript received July 10, 2013; revised July 1, 2014; accepted September 16, 2014. Recommended by Technical Editor H. Ding.

K. Cho, J. Kim, and S. B. Choi are with the Department of Mechanical Engineering, Korea Advanced Institute of Science and Technology, Daejeon 305-701, Korea (e-mail: khcho08@kaist.ac.kr; jjong52@kaist.ac.kr; sbchoi@kaist.ac.kr).

S. Oh is with the Department of Mechanical Engineering, Sogang University, Seoul 121-742, Korea (e-mail: sehoon74@gmail.com).

Color versions of one or more of the figures in this paper are available online at http://ieeexplore.ieee.org.

Digital Object Identifier 10.1109/TMECH.2014.2365996

Q-filter occurs magnitude distortion as well as phase lag of the estimated disturbance since its bandwidth is limited due to high-frequency noise or unmodeled dynamics [19], [20]. Although Luenberger-type DOB without Q-filter is proposed in [21], it is not enough to compensate for time-varying disturbances since it requires accurate model parameters assuming the disturbance is slowly varying.

However, assuming that these disturbances have periodic and repetitive characteristics, the compensation problem can become much easier to handle. In general, all measured states and disturbances in PMLSM motion systems can have the same repetitive time period as that of reference trajectories since the required tasks are periodic and repetitive, and then the stated assumption becomes reasonable. The learning control schemes such as periodic adaptive learning control (PALC), repetitive control (RC), and iterative learning control (ILC) are very effective to attenuate these periodic disturbances without mathematical models. In [22], PALC was proposed to compensate for these periodic disturbances in a PMLM motion system. In [23] and [24], RC was presented to eliminate the periodic tracking error and unmodeled disturbances. In [25] and [26], ILC was presented to enhance the performance of conventional PID feedback control in a PMLM motion system. However, PALC requires complicated nonlinear-function-based design procedures for initial conditions of disturbances to be estimated. In ILC and RC, an inverse model of the closed-loop transfer function should be utilized to design the learning filter guaranteeing the error convergence to zero, and the initial conditions in ILC should be reset [27].

To improve these problems, the authors have proposed a novel disturbance compensation scheme to attenuate periodic disturbances on repetitive motion of PMLSM motion systems in [28] and [29]. This is called the periodic adaptive disturbance observer (PADOB). In the proposed scheme, a lumped disturbance, which includes parametric errors multiplied by states, friction force, and force ripple, is estimated by the DOB for the initial repetitive time period and stored in memory storages. The disturbance is then updated for each time period by the periodic adaptation (PA) law. This scheme requires no mathematical models of friction force and force ripple and adaptation laws of model parameters such as the mass of the mover and viscous friction coefficient. It is also making it possible to compensate for disturbances above as well as within the bandwidth of the Q-filter of the DOB. The proposed design process shows that not only learning control schemes such as ILC and RC can be designed not from the point of view of a control input but disturbances, and also it facilitates the design of the learning filter to guarantee the asymptotical stability. In this paper, more systematic demonstrations of the proposed scheme in [28] and [29] are presented. The experimental verification of the proposed scheme is performed under the reference trajectories considering force ripple and switching friction force. To verify the effectiveness of the proposed scheme, the comparative studies with DOB and RC are also implemented.

This paper is organized as follows. In Section II, the problem formulation of this paper is presented. In Section III, the proposed PADOB is illustrated. The effectiveness of PADOB is verified by various experiments in Section IV. Finally, Section V provides some concluding remarks.

II. Problem Formulation

In this section, a mathematical model of the PMLSM is represented and control problems are defined. Also, the assumptions and properties of states and lumped disturbance are illustrated.

A. PMLSM Model

The comprehensive model of a PMLSM motion system is represented as follows:

$$M\frac{d^2x(t)}{dt^2} = -B\frac{dx(t)}{dt} + F_e(t) - F_{\rm fric}(x,\dot{x}) - F_{\rm rip}(x) \quad (1)$$

where $x(t)$ is the position of the mover, M is the mass of the mover, B is the viscous friction coefficient, $F_e(t)$ is the thrust force, $F_{\rm fric}(x,\dot{x})$ is the friction force, and $F_{\rm rip}(x)$ is the force ripple. For simplicity, the external disturbances and electrical dynamics are ignored because the external disturbance is very small and the electrical dynamics is fast enough comparing with the frequency bandwidth of the interest [30].

Using a nominal model, which has known mass M_n and viscous friction coefficient B_n, (1) is rearranged as follows:

$$M_n\ddot{x}(t) = -B_n\dot{x}(t) + u(t) + d(t) \quad (2)$$

where $u(t)$ is the control input($u(t) = F_e(t) = K_f i_q(t)$), K_f is the force constant, and $i_q(t)$ is the q-axis current.

In (2), $d(t)$ is the lumped disturbance, which includes the friction force, the force ripple, and the parametric errors multiplied by states. It is represented as follows:

$$d(t) = -\Delta M\ddot{x}(t) - \Delta B\dot{x}(t) - F_{\rm fric}(x,\dot{x}) - F_{\rm rip}(x) \quad (3)$$

where $\Delta M = M - M_n$ and $\Delta B = B - B_n$ are the parametric errors of the mass and viscous friction coefficient, respectively.

B. Assumptions and Properties

The control objective is to track the desired position $x_d(t)$ and the corresponding desired velocity $\dot{x}_d(t)$ given for a PMLSM motion system with minimized tracking errors. The required task has the following assumptions.

1) *Assumption 1:* The given task for the PMLSM motion system is to track periodic position trajectories under the same operating conditions repetitively.
2) *Assumption 2:* The effects of disturbances in the PMLSM motion system are identical for each repetitive time period due to no external disturbances.
3) *Assumption 3:* The measurement noise exists mostly in the high-frequency range.

From these assumptions, all the measured states and disturbances have the following properties.

Property 1: (Periodicity of desired and measured states)

From *Assumption 1*, when the desired trajectories that have the repetitive time period P_t are given as follows:

$$x_d(t) = x_d(t-P_t),\ \dot{x}_d(t) = \dot{x}_d(t-P_t),\ \ddot{x}_d(t) = \ddot{x}_d(t-P_t)$$

it can be considered that the measured states are also periodic and they have the same time period P_t if a tracking performance is guaranteed

$$x(t) \approx x(t-P_t),\ \dot{x}(t) \approx \dot{x}(t-P_t),\ \ddot{x}(t) \approx \ddot{x}(t-P_t).$$

Property 2: (Periodicity of disturbance)
From *Assumption 2* and *Property 1*, the lumped disturbance $d(t)$ has the following property due to the state-dependent characteristics:

$$d(t) \approx d(t-P_t).$$

III. Periodic Adaptive Disturbance Observer

In this section, the proposed control scheme PADOB is illustrated in detail that is based on the assumptions and properties addressed in Section II.

A. Design Procedure

The structure of the proposed control scheme is described in Fig. 1, and it is designed by the following two phases:

1) *Searching Phase* ($0 \le t < P_t$):
The system is controlled by a PID feedback controller with a feedforward controller. The lumped disturbance in the low-frequency range is estimated and attenuated by DOB and stored in memory storages.
2) *Learning Phase* ($t \ge P_t$):
The disturbance estimated in the searching phase is utilized as the initial condition for the PA law in PADOB. It is updated by the tracking errors at current time period and minimizes position tracking errors with feedback and feedforward controllers.

B. Searching Phase

First, consider the case when $0 \le t < P_t$. The first block diagram in Fig. 1 presents the structure of the searching phase. The output of the plant with DOB, position $x(t)$, is represented by

$$x(s) = P_n(s)u_r(s) + P_n(s)(1-Q(s))d(s) - Q(s)n(s) \quad (4)$$

where s is the variable in s-domain, $n(s)$ is the sensor noise, $u_r(s) = u_{ff}(s) + u_{fb0}(s)$, and $P_n(s) = 1/(M_n s^2 + B_n s)$. In (4), all the transfer functions are stable and the cutoff frequency of the Q-filter is set to ω_c^Q. Within the frequency bandwidth of the Q-filter (i.e., $|Q(j\omega)| = 1$, $\omega < \omega_c^Q$), the output $x(j\omega)$ becomes similar to $P_n(j\omega)u_r(j\omega) - n(j\omega)$. From *Assumption* 3 (i.e., $n(j\omega) = 0$ at $\omega < \omega_c^Q$), we have the nominal input–output relation as follows:

$$x(j\omega) = P_n(j\omega)u_r(j\omega). \quad (5)$$

It guarantees that the actual plant behaves as the nominal model since the low-frequency components of the lumped disturbance are attenuated by DOB. Therefore, the feedback and feedforward controllers based on the nominal model can be designed. More detailed DOB design methodologies are presented in numerous studies [19], [20].

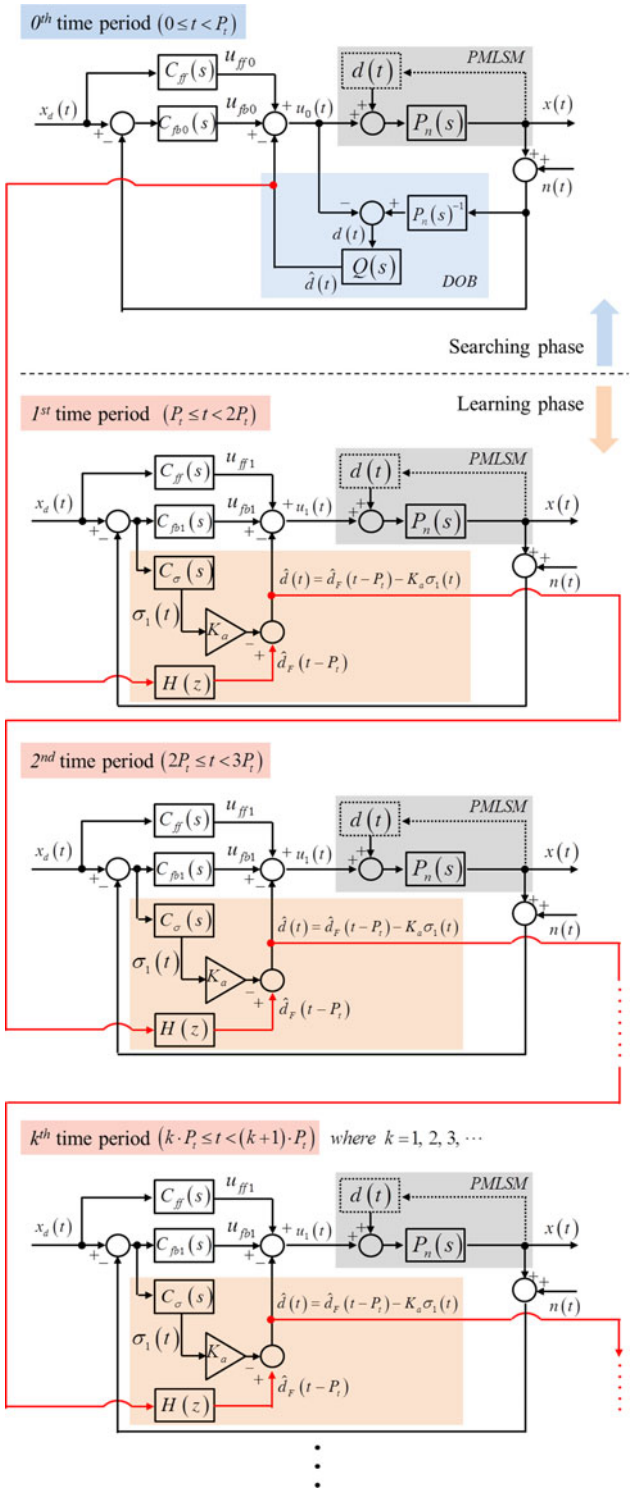

Fig. 1. Block diagram of PADOB.

Based on the nominal model, the control law in the time domain is designed as follows:

$$u_0(t) = u_{ff}(t) + u_{fb0}(t) - \hat{d}(t) \quad (6)$$

$$u_{ff}(t) = M_n\ddot{x}_d(t) + B_n\dot{x}_d(t) \quad (7)$$

$$u_{fb0}(t) = K_{\sigma 0}\sigma_0(t) \tag{8}$$

$$\hat{d}(t) = q(t) * [M_n\ddot{x}(t) + B_n\dot{x}(t) - u(t)] \tag{9}$$

where

$$\sigma_0(t) = \dot{e}_{xF}(t) + a_0 e_x(t) + b_0\int_0^t e_x(r)dr \tag{10}$$

and

$$e_x(t) = x_d(t) - x(t). \tag{11}$$

Here, $u_{ff}(t)$ and $u_{fb0}(t)$ are feedforward and feedback control inputs, $\hat{d}(t)$ is the lumped disturbance that is estimated by DOB, $q(t)$ is the representation of $Q(s)$ in the time domain, and "$*$" is the convolution operation. $K_{\sigma 0}$, a_0, and b_0 are positive tuning parameters.

$\dot{e}_{xF}(t)$ in (10) means the filtered signal of $\dot{e}_x(t)$ by the low-pass filter that has the time constant of τ_L. The mathematical representations between the original and the filtered signals by the low-pass filter $q_L(s)$ in the time domain and the frequency domain are presented as follows:

$$\tau_L\ddot{e}_{xF}(t) = \dot{e}_x(t) - \dot{e}_{xF}(t) \tag{12}$$

$$[se_{xF}(s)] = q_L(s)[se_x(s)] = \frac{1}{\tau_L s + 1}[se_x(s)]. \tag{13}$$

This low-pass filter is utilized to attenuate the amplification of the noise induced by the derivative action.

To prove the stability of the closed-loop system, (2) is rewritten as follows:

$$M_n\ddot{x}(t) = -B_n\dot{x}(t) + u_0(t) + d_l(t) + d_h(t) \tag{14}$$

where $d_l(t)$ and $d_h(t)$ are the low- and high-frequency components of the lumped disturbance in (3), respectively. Substituting (6) into (14), the closed-loop error dynamics is obtained as follows:

$$M_n\ddot{e}_x(t) + B_n\dot{e}_x(t) + K_{\sigma 0}\sigma_0(t) = -d_h(t) - \tilde{d}_l(t) \tag{15}$$

where $\tilde{d}_l(t) = d_l(t) - \hat{d}(t)$ is the estimation error of the low-frequency components of lumped disturbance and it may not be eliminated perfectly due to the phase lag of the Q-filter in DOB. However, since the measured states and high-frequency disturbances such as friction force on speed reversal motion and high-order harmonics of force ripple at high speeds are physically bounded, it can be presented as follows:

$$\left\|d_h(t) + \tilde{d}_l(t)\right\|_\infty < \epsilon, \quad \text{for} \quad \exists\epsilon > 0. \tag{16}$$

In the frequency range below the cutoff frequency of LPFs (i.e., $q_L(j\omega) = 1$ at $\omega < \omega_c^L = 1/\tau_L$), the overall closed-loop transfer function from the remained disturbances to the tracking error is obtained as follows:

$$\frac{e_x(s)}{-d_h(s) - \tilde{d}_l(s)} = \frac{s}{M_n s^3 + (B_n + K_{\sigma 0})s^2 + K_{\sigma 0}a_0 s + K_{\sigma 0}b_0}. \tag{17}$$

In (17), since all desired poles are designed to be located on the left-half plane, the overall system can be stable, while the steady state tracking errors exist.

C. Learning Phase

DOB is known as a powerful method to deal with modeling uncertainties since it compensates perfectly for the parametric errors of the nominal model and disturbances existed within the bandwidth of the Q-filter. However, if dominant uncertainties exist beyond the bandwidth of Q-filter and the phase lag is heavy, then the tracking performance may deteriorate. Thus, parameters of the nominal model should be updated by certain adaptation schemes to minimize parametric errors or the bandwidth of the Q-filter should be widened to include all the frequency components of dominant disturbances within the frequency bandwidth of the interest. However, the method of directly updating parameters of the nominal model may induce instability problems because poles and zeros of the transfer function of the nominal model can be changed irregularly. Also, the bandwidth of Q-filter must be limited due to sensor noise or other unmodeled dynamics, which should not be triggered.

The objective of the learning phase is to compensate for phase lag and magnitude distortion of the disturbance estimated in the searching phase and minimize position tracking errors. From the second block diagram in Fig. 1, the cases when $t \geq P_t$ are shown. The control law in the learning phase is designed as follows:

$$u_1(t) = u_{ff}(t) + u_{fb1}(t) - \hat{d}(t) \tag{18}$$

$$u_{fb1}(t) = K_{\sigma 1}\cdot\sigma_1(t) + (M_n a_1 - B_n)\dot{e}_{xF}(t) + M_n b_1 e_x(t) \tag{19}$$

where

$$\sigma_1(t) = \dot{e}_{xF}(t) + a_1 e_x(t) + b_1\textstyle\int_0^t e_x(r)dr. \tag{20}$$

Here, $u_{ff}(t)$ is the same feedforward control input in (7) and $u_{fb1}(t)$ is the feedback control input. $K_{\sigma 1}$, a_1, and b_1 are positive tuning parameters. In (19) and (20), $\dot{e}_{xF}(t)$ is the filtered signal of $\dot{e}_x(t)$ by the low-pass filter that has the mathematical representations in (12) and (13).

The PA law of the lumped disturbance is designed as follows:

$$\hat{d}(t) = \hat{d}_F(t - P_t) - K_a\sigma_1(t) \tag{21}$$

where

$$\hat{d}_F(t - P_t) = H\left[\hat{d}(t - P_t)\right] = \sum_{k=-n}^{n} c_{|k|}z^{-k}\hat{d}(t - P_t). \tag{22}$$

Here, K_a is an adaptation gain ($K_a > 0$). To prevent the divergence of the estimated lumped disturbance, if $|\hat{d}(t)| > \zeta$, then $K_a = 0$. ζ is the maximum value of the actual lumped disturbance and it is a known value.

$H[\cdot]$ is a zero-phase low-pass filter (ZPF) that has the cutoff frequency of ω_c^H, n is the order of the filter, and z^{-k} is a k-step time delay. $c_{|k|}$ is the normalized coefficient of the filter, and it has a property as $2\sum_{k=1}^{n} c_k + c_0 = 1$. The ZPF is utilized to prevent the adaptation law from learning nonperiodic high-frequency disturbances and to keep the overall system stable from unmodeled dynamics.

In (21) and (22), the disturbance stored in the searching phase is utilized as $\hat{d}(t - P_t)$ when $P_t \leq t < 2P_t$. After the second

time period, the disturbance estimated in the previous time period is utilized as the initial condition of the PA law in the current time period.

To prove the stability of the closed-loop system with the designed controllers and adaptation law, (21) is rewritten as follows:

$$\begin{aligned}\hat{d}(t) =&\ \hat{d}_F(t-P_t) - K_a\sigma_1(t)\\ =&\ \hat{d}(t-P_t) - \hat{d}_h(t-P_t) - K_a\sigma_1(t). \end{aligned} \tag{23}$$

Here, $\hat{d}_h(t-P_t)$ is the high-frequency component of the estimated disturbance at the previous time period that is eliminated by ZPF.

Consider the following positive Lyapunov candidate function:

$$V(t) = \frac{1}{2}\sigma_1^2(t) + \frac{1}{2K_aM_n}\int_{t-P_t}^{t}\tilde{d}^2(r)dr \tag{24}$$

where $\tilde{d}(t) = d(t) - \hat{d}(t)$. Since it can be considered that the periodic disturbance approximated in $Property\ 2$ consists of the dominant periodic and partial nonperiodic components due to $Assumptions$ and $Properties$, the actual disturbance $d(t)$ can be represented as follows:

$$d(t) = d(t-P_t) + d_n(t) \tag{25}$$

where $d_n(t)$ is the nonperiodic disturbance. The disturbances such as unmodeld dynamics, the high-frequency noise and the switching friction force induced by the difference between speed reversal moments at each time period can be considered as $d_n(t)$.

Then, the difference between the positive Lyapunov candidate functions at two discrete time points (t and $t-P_t$) is calculated as follows:

$$\begin{aligned}\Delta V(t) =&\ V(t) - V(t-P_t)\\ =&\ \frac{1}{2}\sigma_1^2(t) - \frac{1}{2}\sigma_1^2(t-P_t)\\ &+ \frac{1}{2K_aM_n}\int_{t-P_t}^{t}\left[\tilde{d}^2(r) - \tilde{d}^2(r-P_t)\right]dr. \end{aligned} \tag{26}$$

For simplicity, let the first two terms at the right-hand side of (26) be denoted by $I_1(t)$ and the integral term by $I_2(t)$. Then, $I_1(t)$ is calculated as follows:

$$\begin{aligned}I_1(t) =&\ \frac{1}{2}\sigma_1^2(t) - \frac{1}{2}\sigma_1^2(t-P_t) = \int_{t-P_t}^{t}\sigma_1(r)\dot{\sigma}_1(r)dr\\ =&\ -\frac{1}{M_n}\int_{t-P_t}^{t}\left[K_{\sigma 1}\sigma_1^2(r) + \tilde{d}(r)\sigma_1(r)\right]dr\\ &+\frac{1}{M_n}\int_{t-P_t}^{t}\sigma_1(r)\tau_L\left[(M_na_1 - B_n)\ddot{e}_{xF}(r)\right.\\ &\left.-M_n\ddot{e}_{xF}(r)\right]dr\\ =&\ -\frac{1}{2K_aM_n}\int_{t-P_t}^{t}[2K_aK_{\sigma 1}\sigma_1^2(r) + 2K_a\tilde{d}(r)\sigma_1(r)]dr\\ &+\frac{1}{2K_aM_n}\int_{t-P_t}^{t}2K_a\sigma_1(r)\epsilon_L(r)dr \end{aligned} \tag{27}$$

where

$$\epsilon_L(r) = \tau_L\left[(M_na_1 - B_n)\ddot{e}_{xF}(r) - M_n\ddot{e}_{xF}(r)\right]. \tag{28}$$

$I_2(t)$ is also calculated as follows:

$$\begin{aligned}I_2(t) =&\ \frac{1}{2K_aM_n}\int_{t-P_t}^{t}\left[\tilde{d}^2(r) - \tilde{d}^2(r-P_t)\right]dr\\ =&\ \frac{1}{2K_aM_n}\int_{t-P_t}^{t}\left[-\{K_a\sigma_1(r) + d_n(r)\}^2\right.\\ &+2K_a\tilde{d}(r)\sigma_1(r)\\ &+2d_n(r)\tilde{d}(r) - \hat{d}_h(r-P_t)\{\hat{d}_h(r-P_t)\\ &\left.-2\tilde{d}(r) + 2K_a\sigma_1(r) + 2d_n(r)\}\right]dr. \end{aligned} \tag{29}$$

From (27) and (29), (26) is rewritten by using Cauchy–Schwarz inequality as follows:

$$\begin{aligned}\Delta V(t) =&\ I_1(t) + I_2(t)\\ =&\ -\frac{1}{2K_aM_n}\int_{t-P_t}^{t}2K_aK_{\sigma 1}\sigma_1^2(r)dr\\ &+\frac{1}{2K_aM_n}\int_{t-P_t}^{t}2K_a\sigma_1(r)\epsilon_L(r)dr\\ &-\frac{1}{2K_aM_n}\int_{t-P_t}^{t}(d_n(r) + K_a\sigma_1(r))^2dr\\ &+\frac{1}{2K_aM_n}\int_{t-P_t}^{t}2d_n(r)\tilde{d}(r)dr\\ &-\frac{1}{2K_aM_n}\int_{t-P_t}^{t}\hat{d}_h(r-P_t)\{\hat{d}_h(r-P_t)\\ &-2\tilde{d}(r) + 2K_a\sigma_1(r) + 2d_n(r)\}dr\\ \le&\ -\frac{1}{2K_aM_n}\int_{t-P_t}^{t}\left[2K_aK_{\sigma 1}\sigma_1^2(r) - 2(K_a\sigma_1(r))^2\right.\\ &\left.-\epsilon_L^2(r) - 2\hat{d}_h^2(r-P_t) - 2d_n^2(r) - 2\tilde{d}^2(r)\right]dr. \end{aligned} \tag{30}$$

Since the time constant of the low-pass filters, τ_L is small enough (i.e., $\tau_L \approx 0$) and the magnitude of the high-frequency components of the estimated disturbances is also very small due to ZPF (i.e., $\hat{d}_h(r-P_t) \approx 0$), following conditions can be guaranteed:

$$|\epsilon_L(t)| < \sqrt{\eta}_1, \quad \eta_1 \ge 0 \tag{31}$$

$$|\hat{d}_h(t-P_t)| < \sqrt{\eta}_2, \quad \eta_2 \ge 0. \tag{32}$$

When the nonperiodic disturbance and the estimation error of the lumped disturbance are bounded as follows:

$$|d_n(t)| < \sqrt{\eta}_3, \quad \eta_3 \ge 0 \tag{33}$$

and

$$|\tilde{d}(t)| < \sqrt{\eta}_4, \quad \eta_4 \ge 0 \tag{34}$$

the difference ΔV becomes as follows:

$$\Delta V(t) < -\frac{1}{2K_a M_n}\int_{t-P_t}^{t}\left[2K_a(K_{\sigma 1}-K_a)\sigma_1^2(r) - \eta_1 - 2\eta_2 - 2\eta_3 - 2\eta_4\right]dr. \quad (35)$$

When the following condition is guaranteed:

$$2K_a(K_{\sigma 1}-K_a)\sigma_1^2(r) \geq \eta \quad (36)$$

where

$$\eta = \eta_1 + 2\eta_2 + 2\eta_3 + 2\eta_4 \quad (37)$$

the difference ΔV becomes negative semidefinite as follows:

$$\Delta V(t) \leq -\frac{1}{2K_a M_n}\int_{t-P_t}^{t}\left[2K_a(K_{\sigma 1} - K_a)\sigma_1^2(r) - \eta\right]dr \leq 0. \quad (38)$$

Here, (36) can be guaranteed by the tracking errors with certain bounded level for any $K_{\sigma 1}$ and K_a. Therefore, it can be proved that the system is stable in the case that there exist the nonperiodic disturbance.

On the other hand, in the case that the effects of the filters such as LPF and ZPF are negligible (i.e., $\tau_L = 0$ and $\hat{d}_h(t - P_t) = 0$) and the actual disturbance is considered as a periodic disturbance (i.e., $d_n(t) = 0$)), the difference $\Delta V(t)$ becomes negative semidefinite as follows:

$$\Delta V(t) = -\frac{1}{2K_a M_n}\int_{t-P_t}^{t}\left[\left(2K_a K_{\sigma 1} + K_a^2\right)\sigma_1^2(r)\right]dr \leq 0. \quad (39)$$

From LaSalle's invariant set theorem, the asymptotical stability of the overall system is proved [31].

D. Gain Design of Feedback Controllers

The gains of the proposed PADOB controller are determined by the following process. In the searching phase, since the actual plant behaves as the nominal model within the frequency bandwidth of the Q-filter due to DOB (i.e., $\omega < \omega_c^Q < \omega_c^L$), the closed-loop dynamics based on the nominal model without disturbance is considered, and it is derived from (10) and (15) as follows:

$$s^3 + \frac{(B_n + K_{\sigma 0})}{M_n}s^2 + \frac{K_{\sigma 0}a_0}{M_n}s + \frac{K_{\sigma 0}b_0}{M_n} = 0. \quad (40)$$

For simplicity of the gain tuning process, all the poles are designed to have the same value. When a desired pole is located at $-p_0$, the control gains are obtained as follows:

$$K_{\sigma 0} = 3M_n p_0 - B_n, \quad a_0 = \frac{3M_n p_0^2}{K_{\sigma 0}}, \quad b_0 = \frac{M_n p_0^3}{K_{\sigma 0}}. \quad (41)$$

In the learning phase, substituting (18) into (2) and assuming that the lumped disturbances can be compensated for by the PA mechanism perfectly, the closed-loop error dynamics within the frequency bandwidth of the interest ($\omega < \omega_c^H < \omega_c^L$) is derived as follows:

$$s^3 + \frac{M_n a_1 + K_{\sigma 1}}{M_n}s^2 + \frac{M_n b_1 + K_{\sigma 1}a_1}{M_n}s + \frac{K_{\sigma 1}b_1}{M_n} = 0. \quad (42)$$

If all poles are located to have the same value at $-p_1$, then the feedback control gains are calculated as follows:

$$K_{\sigma 1} = M_n p_1, \quad a_1 = 2p_1, \quad b_1 = p_1^2. \quad (43)$$

E. Selection of the Adaptation Gain

Here, consider the adaptation gain K_a when the control gains (43) are substituted into (40). Since the desired pole location is determined as $-p_1$, the closed-loop characteristic dynamics with the adaptation law is obtained as follows:

$$M_n(s+p_1)^2\left(s + p_1 + \frac{K_a}{M_n}\right) = 0. \quad (44)$$

If K_a increases, then the system bandwidth can be widened and the transient response is also improved since fast convergence of tracking error to zero is achieved as the learning speed of the disturbance is increased. However, it is impossible to increase the adaptation gain very largely due to the actuator saturation in practice. The large adaptation gain makes not only the overall system more sensitive to unmodeled dynamics that has high-frequency components but also occurs the heavy chattering problem. Therefore, the adaptation gain K_a should be set at a reasonable value to avoid actuator saturation after the desired pole is determined in (44).

To facilitate the selection of the adaptation gain K_a, the relationship between the adaptation gain K_a and convergence speed along the frequency components of the tracking errors to be minimized is considered. To do this work, the transfer function for the error propagation between the current and previous time periods is obtained as follows:

$$T_e = \frac{e_x(t)}{e_x(t-P_t)} = \frac{s+p_1}{s+p_1+K_a/M_n}. \quad (45)$$

When the desired pole p_1 is defined as $\omega_1 = p_1$, the convergence speed to minimize the tracking errors at $\omega < \omega_1$ can be approximated as follows:

$$C_{\mathrm{spd}} = \frac{\omega_1}{\omega_1 + K_a/M_n}. \quad (46)$$

Therefore, the adaptation gain K_a can be determined as follows:

$$K_a = M_n\omega_1\left(\frac{1}{C_{\mathrm{spd}}} - 1\right). \quad (47)$$

In the case of the frequency components of the tracking errors at $\omega_1 < \omega < \omega_1 + K_a/M_n$, the convergence speed to minimize the tracking errors is slower than that at $\omega < \omega_1$ because the transfer function T_e has a slope of 20 dB/dec. At $\omega_1 + K_a/M_n < \omega$, the PA law does not work.

Therefore, the adaptation gain can be determined automatically after the desired pole of the feedback controller $p_1 = \omega_1$ and the convergence speed C_{spd} depending on the frequency components of the tracking errors to be minimized are determined. In the case that the dominant tracking errors have low-frequency components, the large adaptation gain is not required.

On the other hand, the adaptation gain should be increased if the tracking errors that have high-frequency components are dominant, and it will improve the convergence speed to minimize the tracking errors.

However, high-adaptation gain makes the overall system unstable due to high-frequency noise or unmodeled dynamics and occurs the heavy chattering problem. The adaptation gain affects directly the control input and output since it changes the location of the pole in the characteristic equation as shown in (44). To investigate the effect of the adaptation gain K_a on the system stability, the control input and output of the overall system for the tracking errors in Fig. 1 are calculated as follows:

$$u_1(t) = u_1(t - P_t) + T_a(x_d - x - n) \tag{48}$$

and

$$x(t) = x(t - P_t) + T_a(x_d - x - n) \tag{49}$$

where

$$T_a = \frac{K_a C_\sigma}{1 + C_{fb1} P_n} = K_a \frac{s(s + B_n/M_n)}{s + p_1}, \quad B_n/M_n < p_1. \tag{50}$$

The magnitude of the transfer function T_a is increased as the adaptation gain K_a becomes large and the frequency is increased. Therefore, the control input and output become sensitive to the high-frequency noise (or unmodeled output disturbances) due to the derivative action in T_a. To guarantee the stability of the overall system, the adaptation gain K_a must be adjusted as follows.

1) When the reference trajectory requires low speed and acceleration, the magnitude of the control input signal comparing with that of noise (or unmodeled output disturbance) is relative small. The induced disturbances also have low-frequency components because the required motion is slow. Therefore, the overall system can be sensitive to the noise if the large adaptation gain is utilized for this case.
   Since the fast convergence speed is not required, the small adaptation gain is preferred.
2) When the reference trajectory requires high speed and acceleration, the magnitude of the control input signal comparing with that of noise (or unmodeled output disturbance) is relatively large. The induced disturbances have high-frequency components because the required motion is fast. The overall system can be also less sensitive to the noise.
   Since the convergence speed should be increased, the adaptation gain can be increased.

From this analysis, the guideline for the adaptation gain K_a can be illustrated.

IV. Experimental Results

To verify the effectiveness of the proposed control scheme, various real-time experiments considering the force ripple and switching friction force were carried out on the prototype PMLSM motion system shown in Fig. 2. The experimental results of the proposed control scheme were compared with those of other schemes such as RC and PA (which is PADOB without DOB) as well as DOB to evaluate the position tracking performance.

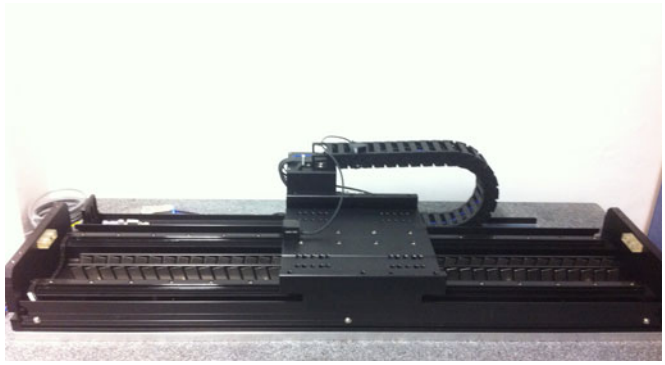

Fig. 2. Experimental PMLSM motion system.

A. Experimental Setup and System Identification

All experiments were carried out based on the prototype PMLSM motion system depicted in Fig. 2. PWM inverter that has 10 kHz switching frequency was utilized and it was controlled by a dSPACE DS1103 board. The current and position controllers were executed at 50 μs and 0.5 ms loop time, respectively. An optical linear encoder, which has a resolution of 0.5 μm, was utilized to measure the position of PMLSM. To guarantee the stability of the overall system, the fourth-order ZPF that has the cutoff frequency of 100 Hz was utilized (i.e., $H(z) = 0.0938z^4 + 0.1064z^3 + 0.1159z^2 + 0.1219z + 0.1240 + 0.1219z^{-1} + 0.1159z^{-2} + 0.1064z^{-3} + 0.0938z^{-4}$).

Since the used PMLSM was a prototype motor, a system identification method based on sine-sweep input signals with various magnitudes was performed to obtain the nominal parameters of this PMLSM. As shown in Fig. 3, various magnitude and phase responses from input q-axis reference current to output speed were obtained. The output speed obtained by the derivative action of the measured position signal was filtered by a low-pass filter. The nominal parameters were determined from the average of these obtained responses, which were presented in Table I.

B. Comparative Studies

To verify the effectiveness of the proposed scheme, following comparative studies are also implemented on the PMLSM motion system.

1) *Disturbance observer:* This controller is same as one in searching phase of PADOB depicted in Fig. 1, which consists of the feedforward controller, PID feedback controller, and DOB. The cutoff frequency of the Q-filter in DOB is well tuned to minimize the tracking errors.
2) *Periodic adaptation:* This controller has the same structure in learning phase of PADOB, but the estimated disturbance is not utilized for the initial condition of the PA law since DOB is not used. So, we define this controller as PA, and it can be considered as a kind of RC (or ILC) with current cycling feedback terms.

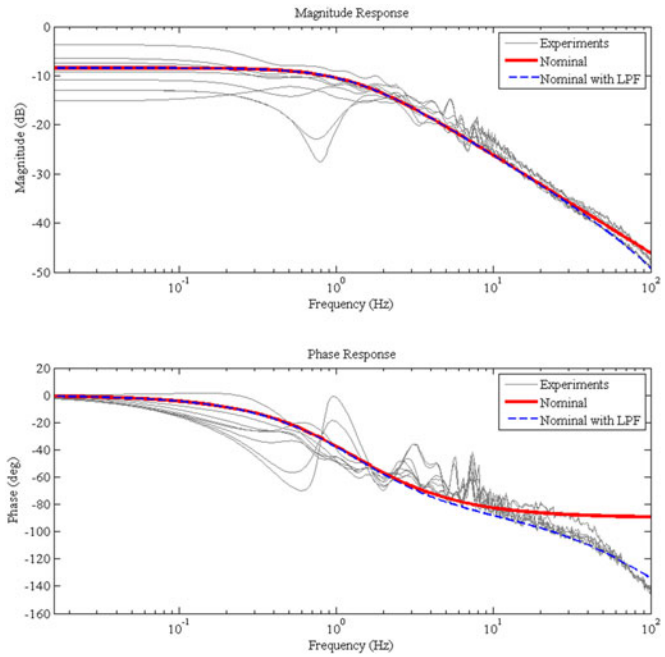

Fig. 3. Frequency response of the PMLSM motion system.

TABLE I
NOMINAL PARAMETERS OF THE PMLSM MOTION SYSTEM

Parameter	Symbol	Value	Unit
Mover mass	M_n	8.70	kg
Viscous friction coefficient	B_n	80.70	N/m/s
Back-emf constant	K_e	25.66	V/m/s
Force constant	K_f	32.98	N/A
Pole pitch	x_p	22.50	mm

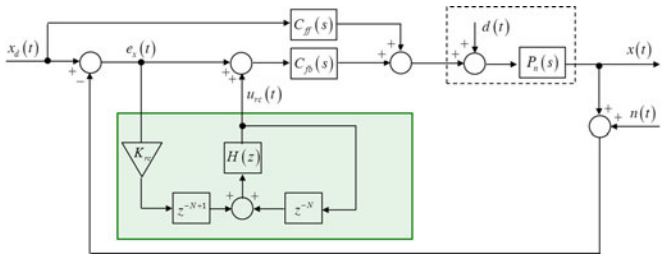

Fig. 4. General repetitive controller for a comparative study (RC).

3) *Repetitive control:* It is a general repetitive controller depicted in Fig. 4, which uses the previous cycling feedback terms. Unlike PADOB and PA, the initial condition of the learning law cannot be utilized since the learning law is designed from the point of view of a control input.

The feedback and feedforward controllers of all the comparative studies are designed identically with those of PADOB. These comparative studies are reasonable to evaluate the tracking performance of the proposed scheme. The comparison of the experimental results of PADOB and DOB shows how the disadvantages of the Q-filter in DOB such as magnitude distortion and phase lag are compensated by the PA law. The performance comparison between the PADOB and PA shows the effectiveness of the initial condition in the learning law designed from the point of view of the disturbance. RC shows the performance comparison along the difference between points of view to design the learning law.

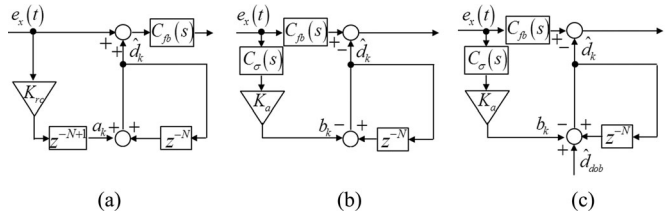

Fig. 5. Simplified structures of learning laws in RC, PA, and PADOB: (a) RC. (b) PA. (c) PADOB.

TABLE II
OUTPUTS OF LEARNING LAWS FOR EACH TIME PERIOD

Time period no.	Outputs	RC	PA	PADOB
0	$\hat{d}_0$	0	b_0	$\hat{d}_{\mathrm{dob}}$
1	$\hat{d}_1$	a_0	b_0+b_1	$\hat{d}_{\mathrm{dob}}+b_1$
2	$\hat{d}_2$	a_0+a_1	$b_0+b_1+b_2$	$\hat{d}_{\mathrm{dob}}+b_1+b_2$
$\vdots$	$\vdots$	$\vdots$	$\vdots$	$\vdots$
k	$\hat{d}_k$	$\sum_{i=0}^{k-1} a_i$	$\sum_{i=0}^{k} b_i$	$\hat{d}_{\mathrm{dob}}+\sum_{i=1}^{k} b_i$

To show the difference between comparative studies clearly, the structures of the learning laws in RC, PA, and PADOB are depicted in Fig. 5. For simplicity, the filters such as LPF and ZPF are omitted and the outputs of all the learning laws are noted as "$\hat{d}_k$." From this figure, the outputs of the learning laws for each controller along the repetitive time period are calculated in Table II. RC has no learning output at the initial time period since it uses only previous cycling feedback terms. PA utilizes the current feedback terms as the learning output at the zeroth time period and it becomes the initial condition at the first time period. In PADOB, the disturbance estimated by DOB is utilized as the learning law at the initial time period, and it is updated periodically by the current feedback terms after the next time period. The differences between PADOB and general ILC/RCs can also be illustrated evidently by these characteristics of learning laws in comparative studies.

C. Evaluation of Tracking Performance for Force Ripple

To evaluate the tracking performance when the force ripple is the dominant disturbance, experiments on repetitive motion under trapezoidal reference position trajectory were carried out. Since the trapezoidal reference position trajectory has repetitive constant speed and stop motions, the fundamental frequency of the force ripple is constant and there is no heavy friction force such as the switching friction force induced at the speed reversal moment. Therefore, the force ripple can be considered as the dominant disturbance on motions. The maximum values of the states of the used reference trajectories are presented in

TABLE III
TRAPEZOIDAL REFERENCE TRAJECTORIES

	Maximum		
	Position$[\mathrm{m}]$	Speed$[\mathrm{m/s}]$	Acceleration$[\mathrm{m/s^2}]$
CASE1	0.06	0.10	2.0
CASE2	0.30	0.50	5.0

TABLE IV
HARMONICS FREQUENCY OF FORCE RIPPLE IN CASE1 AND CASE2

	First freq [Hz]	Second freq [Hz]	Third freq [Hz]	Fourth freq [Hz]	...
CASE1	4.4444	8.8889	13.3333	17.7778	...
CASE2	22.2222	44.4444	66.6667	88.8889	...

Table III. To determine the bandwidth of the Q-filter in DOB and PADOB, the fundamental frequency and its harmonics of the force ripple are calculated in Table IV. The LPF that has the cutoff frequency of 30 Hz was determined as Q-filter for DOB and PADOB. In CASE1, all the dominant components of the force ripple are included in the bandwidth of the Q-filter, while only the fundamental frequency component is within the bandwidth of the Q-filter in CASE2.

Fig. 6(a) shows reference trajectories used for CASE1. The comparison results between PADOB and DOB are shown in Fig. 6(b)–(f). As shown in Fig. 6(b), the tracking performance of DOB was not improved as time goes on (noted as "DOB30"), while the tracking errors of PADOB were decreased due to the PA law (noted as "PADOB700"; $K_a = 700$). Through the results when the adaptation process is completed as depicted in Fig. 6(c) and (d), it was verified that the force ripple was attenuated perfectly in PADOB since the tracking errors were minimized over whole frequency ranges. The improvement of the tracking performance in PADOB was achieved by the PA law that provides the phase lead for the estimated disturbance as shown in Fig. 6(e). However, DOB could not attenuate the force ripple due to phase lag, although the magnitude response of the disturbance estimated by DOB is same as that of the disturbance estimated by PADOB as depicted in Fig. 6(f). Therefore, it is verified that the disadvantage of DOB such as phase lag can be overcome by PADOB. Figs. 6(g)–7 show the experimental results when PADOB is compared with PA and RC. Due to the use of initial condition for the learning law in PADOB, PADOB showed the smallest RMS (root mean square) and MAX (maximum) errors at the zeroth-time period and the fastest error convergence speed among comparative studies. Although the high learning gains are used in PA (noted as "PA900") and RC (noted as "RC04"), the error convergence speeds of PA and RC were not faster than that of PADOB and overall system become even unstable since it is sensitive to unmodeled dynamics and noise due to high learning gains. In Fig. 7, it was verified that the control input of PADOB is nearly the same as other control inputs of the comparative studies when the adaptation process is completed though PADOB guarantees the fastest convergence speed.

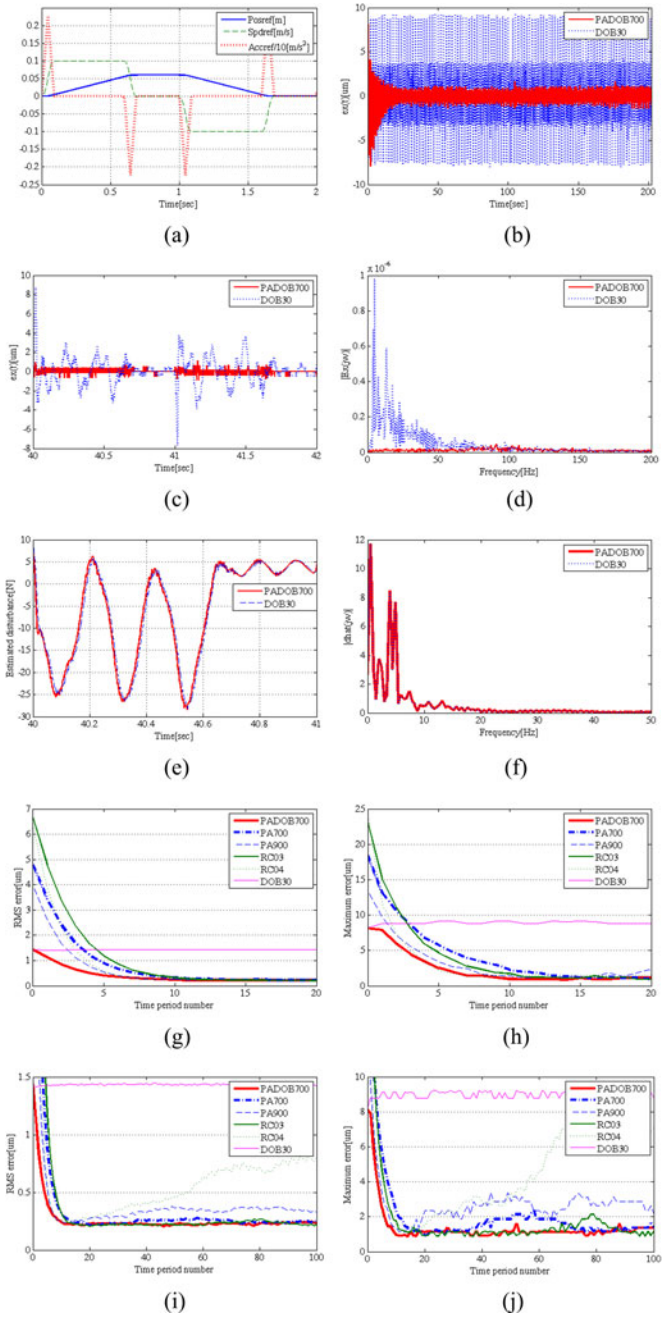

Fig. 6. Tracking performance results in CASE1: (a) Reference trajectories. (b) Position tracking errors for 202 s. (c) Position tracking errors at the 20th time period. (d) FFT results of position tracking errors at the 20th time period. (e) Estimated disturbance at the 20th time period. (f) FFT results of estimated disturbance at the 20th time period. (g) RMS of position tracking errors for 20 time periods. (h) MAX of position tracking errors for 20 time periods. (i) RMS of position tracking errors for 100 time periods. (j) MAX of position tracking errors for 100 time periods.

The experimental results for CASE2 are shown in Fig. 8. Fig. 8(a) shows reference trajectories used for CASE2 and the maximum values of all the states are higher than those of CASE1. In CASE2, since the bandwidth of Q-filter includes only the fundamental frequency of the force ripple, the tracking

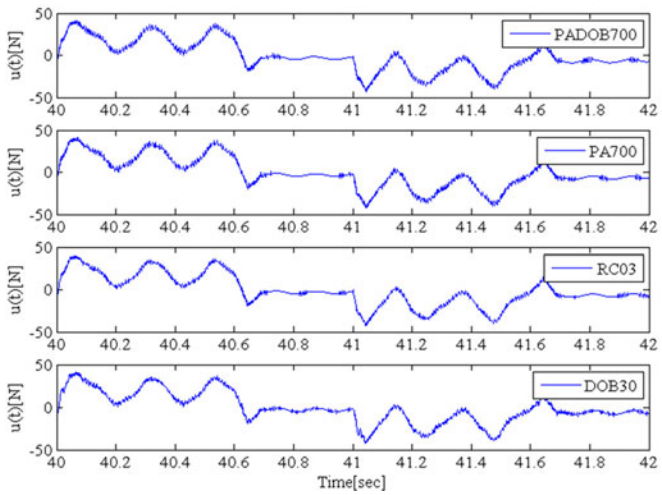

Fig. 7. Control inputs at the 20th time period in CASE1.

performance of DOB was poor as shown in Fig. 8(b)–(d). Unlike CASE1, the magnitude response as well as phase response of the disturbance estimated by DOB were different with those of disturbance estimated by PADOB as depicted in Fig. 8(e) and (f). As the performance of the disturbance estimation in PADOB was improved by the PA law, PADOB showed the superior tracking performance over the whole frequency range. The difference of the RMS and MAX errors at the initial time period between PADOB, PA, and RC was larger than that of CASE1 since the disturbances exist in higher frequency ranges and high-speed/acceleration motion is required. Nevertheless, PADOB showed not only the smallest RMS and MAX errors at the zeroth-time period but also the fastest error convergence speed. Although higher adaptation and learning gains were utilized in PA (noted as "PA1100") and RC (noted as "RC04"), the tracking performances of PA and RC were worse than that of PADOB shown in Fig. 8(i) and (j). As shown in Table V, through the tracking performance results when the adaptation or learning process was completed, it was verified that PADOB shows the best tracking performance with guaranteeing the stability. Furthermore, the control input of PADOB was also a little smaller than those of other controller as shown in Fig. 9. It means that PADOB generates efficient control input since the tracking errors was minimized and the lumped disturbance was estimated very well due to the use of the initial condition of the adaptation law. Therefore, it is verified that PADOB consumes a little less energy while achieving better performance.

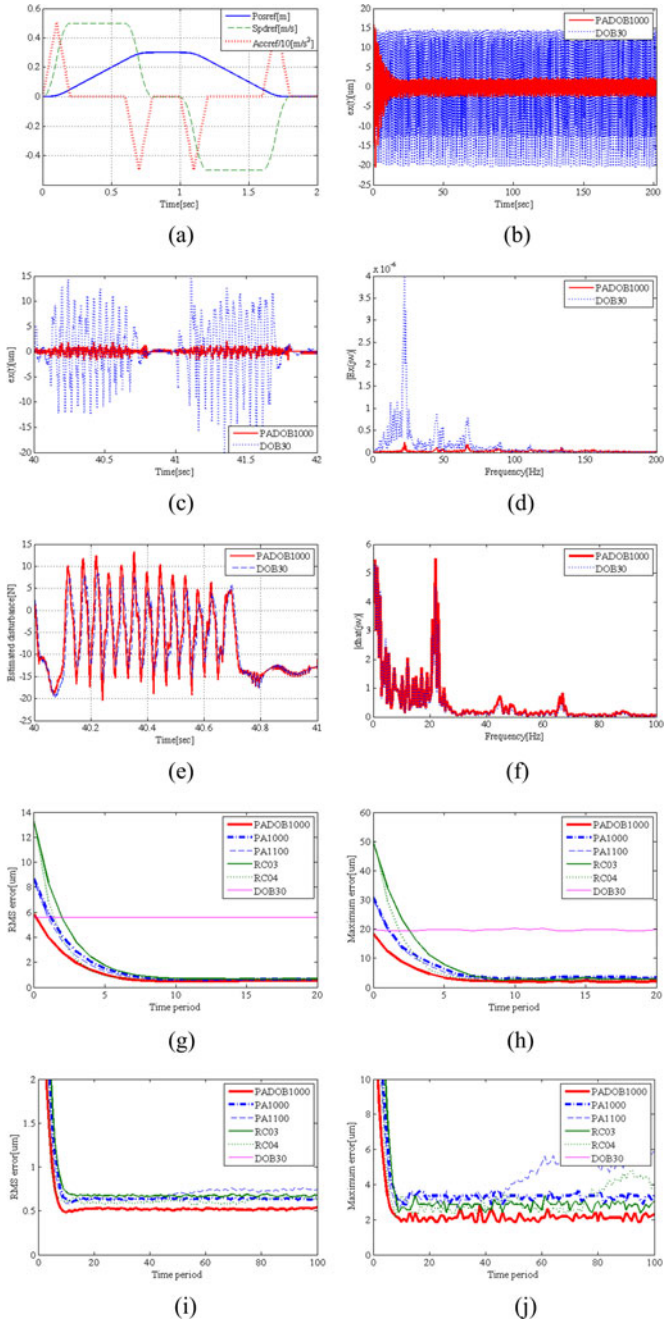

Fig. 8. Tracking performance results in CASE2: (a) Reference trajectories. (b) Position tracking errors for 202 s. (c) Position tracking errors at the 20th time period. (d) FFT results of position tracking errors at the 20th time period. (e) Estimated disturbance at the 20th time period. (f) FFT results of estimated disturbance at the 20th time period. (g) RMS of position tracking errors for 20 time periods. (h) MAX of position tracking errors for 20 time periods. (i) RMS of position tracking errors for 100 time periods. (j) MAX of position tracking errors for 100 time periods.

D. Evaluation of Tracking Performance for Force Ripple and Friction Force

To evaluate the tracking performance of the proposed scheme when the switching friction force as well as the force ripple are existing, experiments under sinusoidal reference trajectory were carried out. Since the sinusoidal trajectories include speed reversal points as well as various operating speed conditions, severe disturbances such as force ripple that has varying fundamental frequencies and the switching friction force are occurred. The used sinusoidal reference trajectories are shown in Table VI. Since maximum speed and acceleration of the reference trajectory in CASE4 are higher than those in CASE3, the case of CASE4 has higher fundamental frequency of force ripple and induces the faster speed reversal motion than those of CASE3. To determine the cutoff frequency of the Q-filter in CASE3 and CASE4, the maximum fundamental frequency and its harmonics

TABLE V
TRACKING PERFORMANCE RESULTS FOR 21∼100 TIME PERIOD IN CASE2

	RMS $\|\|e\|\|_2\,(\mathrm{um})$		MAX $\|\|e\|\|_\infty(\mathrm{um})$	
	average	maximum	average	maximum
PADOB1000	0.5198	0.5401	2.1225	2.8805
PA1000	0.6373	0.6517	3.2915	3.6361
RC03	0.6113	0.6707	3.1424	4.8560

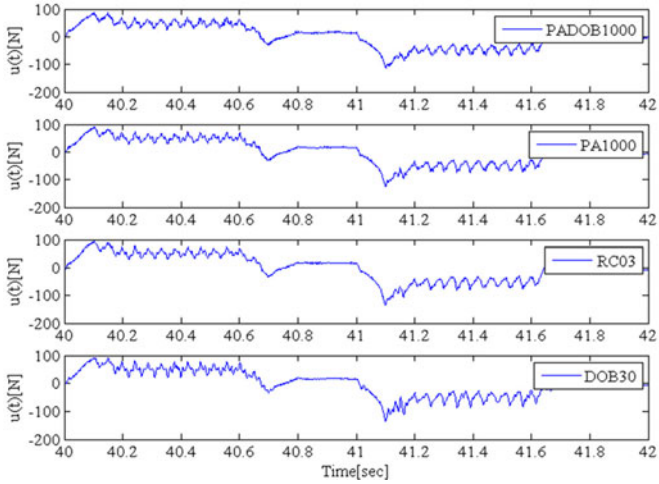

Fig. 9. Control inputs at the 20th time period in CASE2.

TABLE VI
SINUSOIDAL REFERENCE TRAJECTORIES

	Desired Trajectory $x_d\,(t)$	Max Speed [m/s]	Max Accel [m/s^2]
CASE3	$x_d\,(t) = 0.015(1-\cos(\pi t))$	0.0471	0.1480
CASE4	$x_d\,(t) = 0.150(1-\cos(\pi t))$	0.4712	1.4804

TABLE VII
HARMONICS FREQUENCY OF FORCE RIPPLE IN CASE3 AND CASE4

	First freq [Hz]	Second freq [Hz]	Third freq [Hz]	Fourth freq [Hz]	...
CASE3	2.0944	4.1888	6.2832	8.3776	...
CASE4	20.9440	41.8879	62.8319	83.7758	...

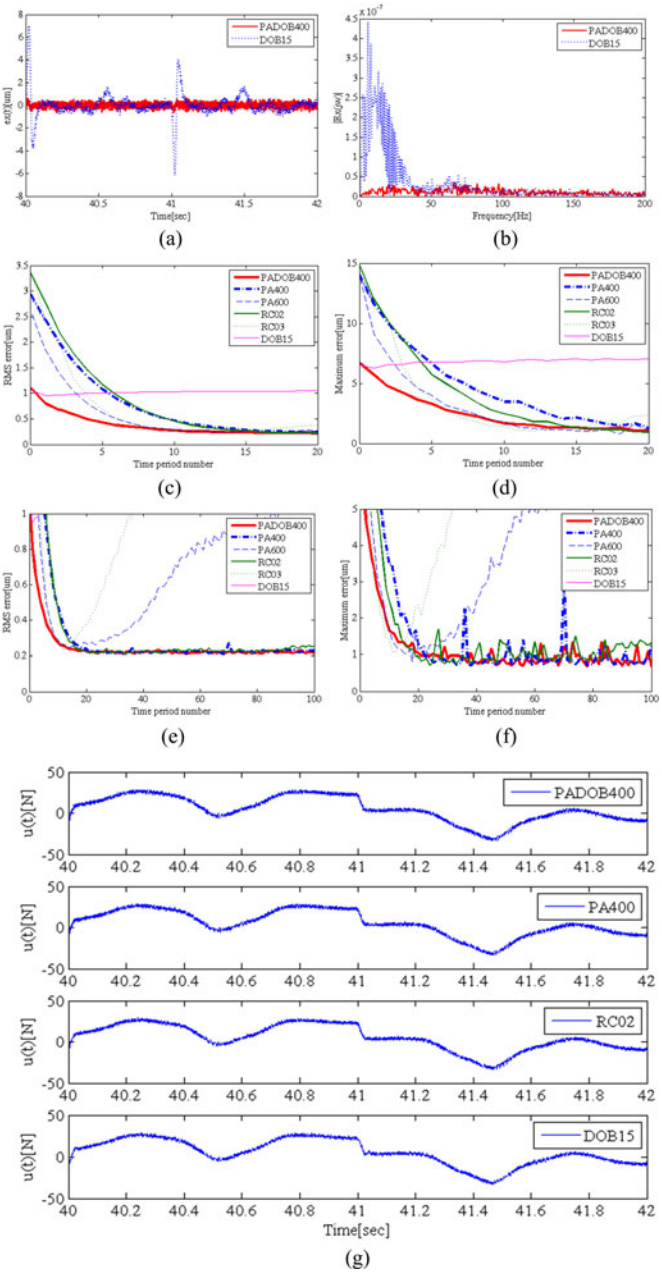

Fig. 10. Tracking performance results in CASE3: (a) Position tracking errors at the 20th time period. (b) FFT results of position tracking errors at the 20th time period. (c) RMS of position tracking errors for 20 time periods. (d) MAX of position tracking errors for 20 time periods. (e) RMS of position tracking errors for 100 time periods. (f) MAX of position tracking errors for 100 time periods. (g) Control inputs at the 20th time period.

of force ripple are calculated as in Table VII when the PMLSM is moving at the maximum speed on the given trajectories. From the calculated results and experimental fine-tuning, the cutoff frequencies of the Q-filter for DOB and PADOB have been selected as 15 and 30 Hz in CASE3 and CASE4, respectively.

The experimental results of the proposed scheme and other comparative studies for CASE3 are shown in Fig. 10. The comparison results between PADOB400 (which uses $K_a = 400$) and DOB15 when the adaptation process is completed are shown in Fig. 10(a) and (b). The tracking performance of DOB15 was worse than that of PADOB400 although all the dominant frequency components of the force ripple were within the bandwidth of the Q-filter. Especially, it was verified that the tracking errors at the speed reversal moment were very large and the force ripple was also not attenuated perfectly. On the other hand, the tracking errors of PADOB400 were minimized over whole frequency range due to the PA law. Fig. 10(c)–(f) shows RMS and MAX tracking errors for each repetitive time period of comparative studies. As shown in these figures, PADOB400 shows the fastest error convergence speed of comparative studies due

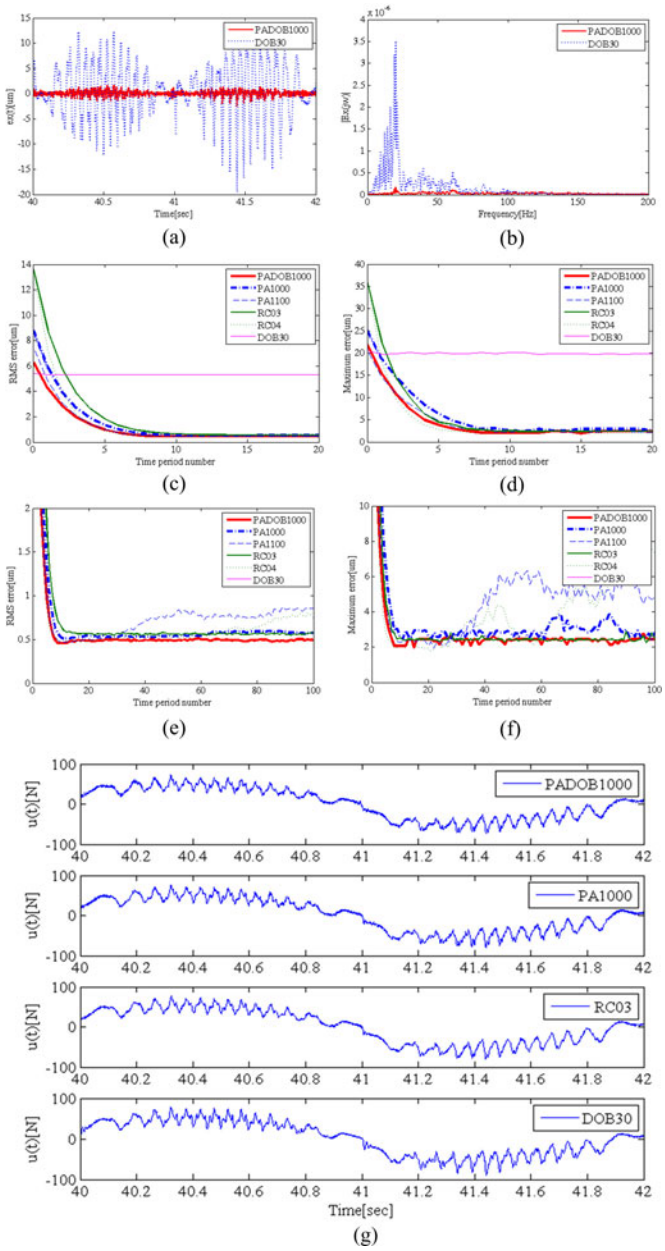

Fig. 11. Tracking performance results in CASE4: (a) Position tracking errors at the 20th time period. (b) FFT results of position tracking errors at the 20th time period. (c) RMS of position tracking errors for 20 time periods. (d) MAX of position tracking errors for 20 time periods. (e) RMS of position tracking errors for 100 time periods. (f) MAX of position tracking errors for 100 time periods. (g) Control inputs at the 20th time period.

to the use of DOB at the initial repetitive time period. In PA and RC, the instability problem was occurred although the error convergence speeds were increased when the high learning gain values were utilized (noted as "RC03" and "PA600"). As shown in Fig. 10(e) and (f), the high gain makes the overall system more sensitive to unmodeled dynamics and noise. Fig. 10(g) shows that the control input of PADOB is nearly the same as other control inputs of the comparative studies when the adaptation process is completed though PADOB guarantees the fastest convergence speed to minimize the tracking errors.

TABLE VIII
TRACKING PERFORMANCE RESULTS FOR 21∼100 TIME PERIOD IN CASE4

	RMS $\|\|e\|\|_2(\mathrm{um})$		MAX $\|\|e\|\|_\infty(\mathrm{um})$	
	average	maximum	average	maximum
PADOB1000	0.4923	0.5095	2.3987	2.7693
PA1000	0.5598	0.5974	2.9126	3.8716
RC03	0.5632	0.5792	2.4375	2.8889

The experimental results of CASE4 are shown in Fig. 11. In CASE4, since only the fundamental frequency component of the force ripple is included in the bandwidth of the Q-filter and the speed reversal motion occurs more fastly than CASE3, DOB was insufficient to attenuate disturbances as shown in Fig. 11(a)–(b). However, PADOB1000 showed that the switching force as well as the force ripple were attenuated effectively through the minimized tracking errors over whole frequency ranges since the PA law in PADOB1000 compensated for the phase lag, magnitude, and high-frequency components of the disturbance estimated by DOB. As in CASE3, PADOB1000 had the smallest RMS and MAX error at the initial repetitive time period when it was compared with PA and RC and showed fast error convergence speed, as depicted in Fig. 11(c) and (d). Through 11(e), (f), and Table VIII, it was also verified that PADOB showed the best tracking performance when the adaptation or learning process is completed. In Fig. 11(g), PADOB showed that the best tracking performance can be guaranteed by a little smaller control input when it is compared with those of comparative studies due to several advantages of PADOB.

From these results, it was verified that the perfect tracking performance can be achieved by PADOB with efficient control input although there exist high-frequency components of disturbances such as switching friction force as well as the force ripple that has varying fundamental frequency.

V. CONCLUSION

In this paper, a novel disturbance compensation scheme to attenuate periodic disturbances on repetitive motion trajectories using a PMLSM motion system has been developed. In the proposed control scheme, it has been proved theoretically that position tracking errors converge to zero asymptotically assuming that all measured states and disturbances have the same repetitive time period as that of reference trajectories. This scheme requires no mathematical models of disturbances or adaptation laws of model parameters such as the mass of the mover and viscous friction coefficient. All the disturbances are attenuated effectively by a periodical adaptation law without separating each disturbance from the lumped disturbance. It is possible to compensate for the disturbances whose frequency components are below and above the bandwidth of the Q-filter of the DOB. Also, it shows that learning control schemes such as ILC and RC can be designed not from the point of view of a control input but disturbances. Through various experiments under reference trajectories considering force ripple and friction force, the proposed control scheme has shown superior position

tracking performance than comparative studies such as DOB, RC, and PA.

However, the systemic design procedure to choose optimal adaptation gain values has not been discussed. As future works, how to determine the optimal gain guaranteeing the stability of the overall system with the best tracking performance will be explored. Also, the proposed scheme has a disadvantage that huge amount of memory is required when the time period of the reference trajectories P_t is very large. This problem becomes less troublesome as the price of the memory continues to decrease these days, but, it is still an important issue in the industrial applications that the cost of production is very important. In the proposed scheme, this problem may be improved by increasing the loop time of the position controller since the total number of samples to be utilized for the periodic feedback is determined as $N = P_t/T_s$ (where T_s is the loop time of the position controller). However, the large loop time makes the tracking performance worse since the time to measure the position signal becomes slow and the samples to estimate the lumped disturbance are not enough. Therefore, the research to minimize the amount of memory will be also performed to improve the practical implementation issue of the proposed scheme as future works.

REFERENCES

[1] K. Tan, T. Lee, S. Huang, and X. Jiang, "Friction modeling and adaptive compensation using a relay feedback approach," *IEEE Trans. Ind. Electron.*, vol. 48, no. 1, pp. 169–176, Feb. 2001.

[2] S.-L. Chen, K. K. Tan, and S. Huang, "Friction modeling and compensation of servomechanical systems with dual-relay feedback approach," *IEEE Trans. Control Syst. Technol.*, vol. 17, no. 6, pp. 1295–1305, Nov. 2009.

[3] C.-I. Huang and L.-C. Fu, "Adaptive approach to motion controller of linear induction motor with friction compensation," *IEEE/ASME Trans. Mechatronics*, vol. 12, no. 4, pp. 480–490, Aug. 2007.

[4] J. Yao, Z. Jiao, and B. Yao, "Robust control for static loading of electro-hydraulic load simulator with friction compensation," *Chin. J. Aeronaut.*, vol. 25, no. 6, pp. 954–962, 2012.

[5] T. H. Lee, K. K. Tan, and S. Huang, "Adaptive friction compensation with a dynamical friction model," *IEEE/ASME Trans. Mechatronics*, vol. 16, no. 1, pp. 133–140, Jan. 2011.

[6] W. Shang and S. Cong, "Motion control of parallel manipulators using acceleration feedback," *IEEE Trans. Control Syst. Technol.*, vol. 22, no. 1, pp. 314–321, Jan. 2014.

[7] C.-J. Lin, H.-T. Yau, and Y.-C. Tian, "Identification and compensation of nonlinear friction characteristics and precision control for a linear motor stage," *IEEE/ASME Trans. Mechatronics*, vol. 18, no. 4, pp. 1385–1396, Jul. 2013.

[8] J. Yao, Z. Jiao, D. Ma, and L. Yan, "High-accuracy tracking control of hydraulic rotary actuators with modeling uncertainties," *IEEE/ASME Trans. Mechatronics*, vol. 19, no. 2, pp. 633–641, Apr. 2014.

[9] T.-S. Hwang and J.-K. Seok, "Observer-based ripple force compensation for linear hybrid stepping motor drives," *IEEE Trans. Ind. Electron.*, vol. 54, no. 5, pp. 2417–2424, Oct. 2007.

[10] L. Bascetta, P. Rocco, and G. Magnani, "Force ripple compensation in linear motors based on closed-loop position-dependent identification," *IEEE/ASME Trans. Mechatronics*, vol. 15, no. 3, pp. 349–359, Apr. 2010.

[11] K. Tan, S. Huang, and T. Lee, "Robust adaptive numerical compensation for friction and force ripple in permanent-magnet linear motors," *IEEE Trans. Magn.*, vol. 38, no. 1, pp. 221–228, Aug. 2002.

[12] L. Lu, Z. Chen, B. Yao, and Q. Wang, "Desired compensation adaptive robust control of a linear-motor-driven precision industrial gantry with improved cogging force compensation," *IEEE/ASME Trans. Mechatronics*, vol. 13, no. 6, pp. 617–624, Dec. 2008.

[13] B. Yao, "Advanced motion control: From classical PID to nonlinear adaptive robust control," in *Proc. IEEE 11th Int. Workshop Adv. Motion Control,* 2010, pp. 815–829.

[14] Z. Chen, B. Yao, and Q. Wang, "Accurate motion control of linear motors with adaptive robust compensation of nonlinear electromagnetic field effect," *IEEE/ASME Trans. Mechatronics*, vol. 18, no. 3, pp. 1122–1129, Jan. 2013.

[15] C. Hu, B. Yao, and Q. Wang, "Performance-oriented adaptive robust control of a class of nonlinear systems preceded by unknown dead zone with comparative experimental results," *IEEE/ASME Trans. Mechatronics*, vol. 18, no. 1, pp. 178–189, Feb. 2013.

[16] K. K. Tan, T. H. Lee, H. F. Dou, S. J. Chin, and S. Zhao, "Precision motion control with disturbance observer for pulsewidth-modulated-driven permanent-magnet linear motors," *IEEE Trans. Magn.*, vol. 39, no. 3, pp. 1813–1818, May 2003.

[17] P. Hamelin, P. Bigras, J. Beaudry, P. Richard, and M. Blain, "Discrete-time state feedback with velocity estimation using a dual observer: application to an underwater direct-drive grinding robot," *IEEE/ASME Trans. Mechatronics*, vol. 17, no. 1, pp. 187–191, Feb. 2012.

[18] R.-J. Liu, M. Wu, G.-P. Liu, J. She, and C. Thomas, "Active disturbance rejection control based on an improved equivalent-input-disturbance approach," *IEEE/ASME Trans. Mechatronics*, vol. 18, no. 4, pp. 1410–1413, Jul. 2013.

[19] T. Umeno and Y. Hori, "Robust speed control of dc servomotors using modern two degrees-of-freedom controller design," *IEEE Trans. Ind. Electron.*, vol. 38, no. 5, pp. 363–368, Oct. 1991.

[20] M. Tomizuka, "Model based prediction, preview and robust controls in motion control systems," in *Proc. 4th Int. Workshop Adv. Motion Control,* 1996, vol. 1, pp. 1–6.

[21] H. Fujimoto, F. Kawakami, and S. Kondo, "Repetitive control of hard disk drives based on switching scheme: Experimental verification for multiple mode disturbance," in *Proc. IEEE 8th Int. Workshop Adv. Motion Control,* 2004, pp. 323–328.

[22] H. Ahn, Y. Chen, and H. Dou, "State-periodic adaptive compensation of cogging and coulomb friction in permanent-magnet linear motors," *IEEE Trans. Magn.*, vol. 41, no. 1, pp. 90–98, Jan. 2005.

[23] S. Chen and T. Hsieh, "Repetitive control design and implementation for linear motor machine tool," *Int. J. Mach. Tools Manuf.*, vol. 47, no. 12, pp. 1807–1816, 2007.

[24] Y. Li and Q. Xu, "Design and robust repetitive control of a new parallel-kinematic xy piezostage for micro/nanomanipulation," *IEEE/ASME Trans. Mechatronics*, vol. 17, no. 6, pp. 1120–1132, Dec. 2012.

[25] T. Lee, K. K. Tan, S. Lim, and H. Dou, "Iterative learning control of permanent magnet linear motor with relay automatic tuning," *Mechatronics*, vol. 10, no. 1, pp. 169–190, 2000.

[26] K. K. Tan, H. Dou, Y. Chen, and T. H. Lee, "High precision linear motor control via relay-tuning and iterative learning based on zero-phase filtering," *IEEE Trans. Control Syst. Technol.*, vol. 9, no. 2, pp. 244–253, Mar. 2001.

[27] M.-S. Tsai, C.-L. Yen, and H.-T. Yau, "Integration of an empirical mode decomposition algorithm with iterative learning control for high-precision machining," *IEEE/ASME Trans. Mechatronics*, vol. 18, no. 3, pp. 878–886, Jun. 2013.

[28] K. Cho, H. Park, S. Choi, and S. Oh, "Precision motion control based on a periodic adaptive disturbance observer," in *Proc. 38th Annu. Conf. IEEE Ind. Electron. Soc.*, 2012, pp. 3832–3837.

[29] K. Cho, J. Kim, H. Park, and S. Choi, "Periodic adaptive disturbance observer for a permanent magnet linear synchronous motor," in *Proc. IEEE 51st Annu. Conf. Decision Control*, 2012, pp. 4684–4689.

[30] J. Yao, Z. Jiao, and D. Ma, "Adaptive robust control of dc motors with extended state observer," *IEEE Trans. Ind. Electron.*, vol. 61, no. 7, pp. 3630–3637, Jul. 2014.

[31] H. Khalil and J. Grizzle, *Nonlinear Systems*. New York, NY, USA: Macmillan, 1992.

Kwanghyun Cho (S'11) received the B.S. degree in electrical engineering and computer science from Kyungpook National University, Daegu, Korea, in 2008, and the M.S., and Ph. D degrees in mechanical engineering from the Korea Advanced Institute of Science and Technology, Daejeon, Korea, in 2010 and 2014.

His research interests include in precision motion control based on linear motors.

Jonghwa Kim received the B.S. degree in materials engineering from Hokkaido University, Sapporo, Japan, in 2006, and the M.S. degree in mechanical engineering from the Korea Advanced Institute of Science and Technology, Daejeon, Korea in 2009.

His research interests include control theory and its application.

Seibum Ben Choi (M'09) received the B.S. degree in mechanical engineering from Seoul National University, Seoul, Korea, in 1985, and the M.S. degree in mechanical engineering from the Korea Advanced Institute of Science and Technology (KAIST), Seoul, Korea in 1987, and the Ph.D degree in controls from the University of California, Berkeley, CA, USA, in 1993.

From 1993 to 1997, he was involved in the development of automated vehicle control systems at the Institute of Transportation Studies, University of California. During 2006, he was with TRW,Warren, MI, USA, where he was involved in the development of advanced vehicle control systems. Since 2006, he has been with the Faculty of the Mechanical Engineering Department, KAIST. His current research interests include fuel-saving technology, vehicle dynamics and control, and active safety systems.

Sehoon Oh (S'05–M'06) received the B.S., M.S., and Ph.D. degrees in electrical engineering from The University of Tokyo, Tokyo, Japan, in 1998, 2000, and 2005, respectively.

He was an Assistant Professor at The University of Tokyo until 2012, and was a Senior Researcher at Samsung Heavy Industries from 2012 to 2013. He was a Visiting Researcher at the University of Texas at Austin from 2010 to 2011. He is currently a Research Professor at Sogang University, Seoul, Korea.

His research interests include the development of human-friendly motion control algorithms and assistive devices for people.